J Electroceram (2007) 18:149–154
DOI 10.1007/s10832-007-9017-6

Preparation of sol-gel-derived $Ca_{1-x}Sr_xZrO_3$ perovskite dielectric thin films

T. Yu · C. H. Chen · Y. K. Lu · X. F. Chen · W. Zhu ·
R. G. Krishnan

Received: 16 February 2004 / Accepted: 27 December 2006 / Published online: 30 March 2007
© Springer Science + Business Media, LLC 2007

Abstract The sol-gel wet chemical synthesis of dielectric thin films of perovskite $Ca_{1-x}Sr_xZrO_3$ has been studied in detail using different techniques. To the best of our knowledge, it is the first time in the literature to systemically study the properties of $Ca_{1-x}Sr_xZrO_3$ dielectric thin films in the whole solid solution composition range. Based on X-ray diffraction (XRD), Flourier transform infrared (FT-IR) reflectivity spectroscopy and atomic force microscope (AFM) data, the mechanisms of $Ca_{1-x}Sr_xZrO_3$ phase transformation and crystallinity have been investigated. The results show that the film annealed at 550 °C is amorphous with existing of carbonates, while the carbonates and other organics are decomposed at 600 °C and above, and the film is crystallized into the perovskite phase with increasing annealing temperature. The values of dielectric constant in a range of 16–30 for $Ca_{1-x}Sr_xZrO_3$ thin films have been obtained. Measured dielectric properties show that those films exhibit stable dielectric properties nearly independent on the applied electrical field and frequency at room temperature. Based on above data, it can be concluded that $Ca_{1-x}Sr_xZrO_3$ thin films are a promising candidate system for the high-k microelectronic devices application.

Keywords Sol-gel · Thin films · XRD · Perovskite

T. Yu (✉) · C. H. Chen · Y. K. Lu · X. F. Chen · W. Zhu
Microelectronics Center, School of Electrical and Electronic Engineering, Nanyang Technological University,
639798 Singapore, Singapore
e-mail: pg01009507@ntu.edu.sg

R. G. Krishnan
Singapore Institute of Microelectronics,
11 Science Park Road, 117685 Singapore, Singapore

1 Introduction

Aggressive dimension scaling of semiconductor devices requires the conventional gate dielectric thickness must also decrease to maintain a given storage capacitance to reduce short-channel effects and to keep device drive current at an acceptable level. Since direct tunneling increases exponentially with decreasing the oxide thickness, continuous scaling of thermal silicon oxide as the gate dielectric has run into difficulties when the oxide thickness is less than 20 Å [1]. The evolving decrease of the gate dielectric film thickness to an oxide-equivalent value of 10 Å is identified as a critical front-end technology issue in the Semiconductor Industry Association's (SIA's) ITRS. A suitable replacement gate dielectric with a high permittivity must exhibit low leakage current, compatibility with CMOS process flow, and exhibit at least the same equivalent capacitance, performance and reliability of silicon oxide. In recent years metal oxides with the ABO_3 perovskite structure are of fundamental interest and significance, as their properties may be tailored to specific applications by subtle changes in chemical doping at A or B cation sites. Perovskite oxides have received great attention recently as high-temperature proton conductors [2, 3]. Alkaline-earth zirconates (such as $CaZrO_3$) are in general chemically stable and have high dielectric constant. Due to its high relative permittivity and low leakage current compared to other dielectric materials, the solid perovskite phase $Ca_xSr_{1-x}ZrO_3$ maybe is one of the promising candidates for use as an alternative dielectric material replacing the conventional silicon oxide in advanced CMOS technologies, and in other integrated capacitor applications. Despite recent structural and synthesis studies [4, 5], there is still a lack of the fundamental understanding of the effects of cation doping in this system. In order to understand the properties of the $(Ca_xSr_{1-x})ZrO_3$ solid

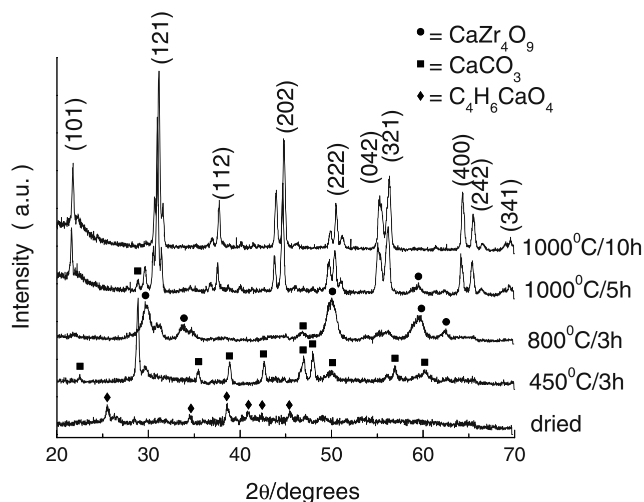

Fig. 1 XRD patterns of the $Ca_{1-x}Sr_xZrO_3$ (x=0) precursor calcined at different temperatures between 150 and 1000 °C

solution system in more detail, in this paper we report our systematic investigation on preparation of this system by using sol-gel technology and characterizations by differential thermal analysis (DTA), thermogravimetric analysis (TGA), X-ray diffraction (XRD), atomic force microscope (AFM) and Auger spectra (AES), and the electric and dielectric properties of these $Ca_{1-x}Sr_xZrO_3$ thin films are also presented and discussed. To the best of our knowledge, it is the first attempt in the literature to systematically study the mechanism of phase transformation and crystallinity, the dielectric properties of the whole $Ca_{1-x}Sr_xZrO_3$ solid solution system, and to seek a possible application for high-k dielectric capacitors.

2 Experimental details

The sol-gel solution was prepared by mixing strontium acetate, calcium acetate and zirconium butoxide dissolved in glacial acetic acid and a small quantity of water. The resulting mixture was sealed in a container and stirred continuously at room temperature until a transparent solution formed through two simultaneous chemical processes, hydrolysis and polymerization. The solution was then spin-coated onto Pt(150 nm)/Ti(150 nm)/SiO_2(500 nm)/Si substrates at a speed of 4,000 rpm to form sol-gel films. Subsequent annealing procedure was carried out on these as-grown films by varying heating temperatures. Film thickness was measured by a Dektak III profiler. XRD analysis was used to study the different phases in the calcined precursors at temperatures between 150 and 1,000 °C and to investigate the crystalline structure of $Ca_{1-x}Sr_xZrO_3$ thin films. The diffraction patterns were obtained by the Bragg–Brentano (θ–2θ) method with Cu $K\alpha$ radiation (λ=1.542 Å). Changes in the oxide growth during the annealing process were investigated by Fourier transform infrared (FTIR) spectroscopy. The electrical properties (*I–V*, *C–V*) of these films were measured by HP4155 and HP4284 semiconductor systems on Pt/$Ca_{1-x}Sr_xZrO_3$/Pt capacitor test structures (Pt top electrode area: 9×10^{-4} cm^2).

3 Results and discussion

Figure 1 shows the XRD spectra taken after calcining the $Ca_{1-x}Sr_xZrO_3$ (x=0) precursor at 150 (1 h) (drying), 450 (3 h), 800 (3 h), 1,000 (5 h), 1,000 °C (10 h). All peaks with ♦ mark observed for the dried precursor can be attributed to calcium acetate ($C_4H_6CaO_4$). If the precursor is calcined at 450 °C, the calcium acetate complexes decompose to $CaCO_3$, confirming the experimental results from the TGA-DTA measurements. In the precursor calcined at 800 °C, two different phases are identified, a $CaZrO_3$ perovskite phase and a $CaZr_4O_9$ cubic phase. Several authors have reported the coexistence of a $CaZrO_3$ perovskite and a $CaZr_4O_9$ cubic phase in the CaO–ZrO_2 system at temperatures up to 1,300 °C with CaO concentrations between 20 and 50 mol% [6–10]. If the precipitated precursor is calcined at 1,000 °C, then the solid-state reactions progress even further towards formation of the desired $CaZrO_3$ phase, as shown in Fig. 1 of the XRD pattern obtained after calcining the precursor for 5 h at 1,000 °C. It can be easily seen that the XRD peaks of the $CaZrO_3$ perovskite phase have increased in intensity. The intensity of the $CaZr_4O_9$ phase has decreased dramatically, indicating a substantial decrease in the amount of this phase. If the precursor is calcined at 1,000 °C for 10 h, the conversion to $CaZrO_3$ phase progresses further and the $CaZr_4O_9$ phase nearly can not be detected.

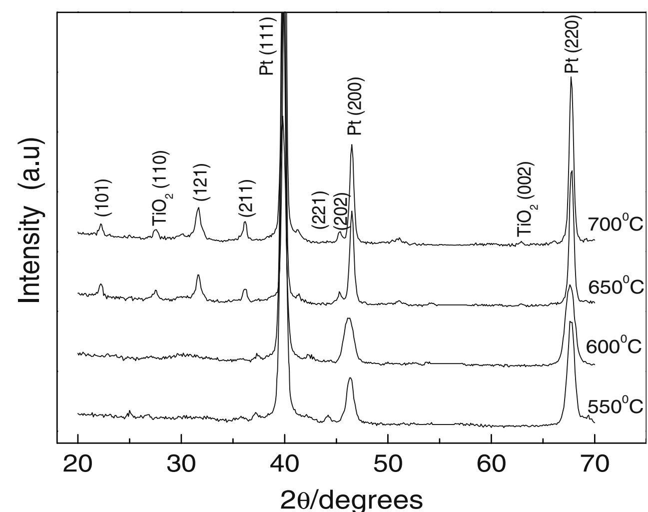

Fig. 2 XRD patterns of the $Ca_{1-x}Sr_xZrO_3$ (x=0) films prepared on Pt/Ti/SiO_2/Si substrates annealed at different temperatures in flowing O_2

The XRD patterns given in Fig. 2 show the crystallization progress of $Ca_{1-x}Sr_xZrO_3$ (x=0) thin films prepared on Pt/Ti/SiO_2/Si substrate and annealed at various temperatures (550, 600, 650 and 700 °C) for 1 h in flowing oxygen. It is clearly shown that the film annealed at 550 °C, which is much lower than the crystallization temperature, indicates that the film has its amorphous structure. As annealing temperature increases to and above 600 °C, the intensity of perovskite $CaZrO_3$ phase is increased, indicating that the further crystallization progress in $CaZrO_3$ thin films. It reveals that the Pt surface can enhance the heteronucleation and growth of the film, and this phenomenon was observed for other materials annealing on Pt coated substrates [11, 12].

The systematic XRD patterns of $Ca_{1-x}Sr_xZrO_3$ ($0 \le x \le 1$) thin films annealed at 700 °C are shown in Fig. 3. It is evident that the XRD profiles of $Ca_{1-x}Sr_xZrO_3$ change systematically with doping x. The strongest diffraction peak of the perovskite phase shifts to the high degree from $SrZrO_3$ (x=1.0) to $CaZrO_3$ (x=0). This is due to the lattice contraction as Sr is replaced by Ca with a smaller ionic radius in $Ca_{1-x}Sr_xZrO_3$. The XRD profiles of each end member $SrZrO_3$ or $CaZrO_3$ can be indexed as orthorhombic unit cell. The lattice parameters are determined to be a=5.879 Å, b=8.147 Å and c=5.769 Å for $SrZrO_3$ (JCPDS 10-0268), and a=5.642 Å, b=7.970 Å and c=5.650 Å for $CaZrO_3$ (JCPDS 35-0790). It also can be seen that the peaks associated with the TiO_2 phase keep constant with the composition x changes.

A bare silicon substrate was used as the reference. The FT-IR reflectivity spectra of those annealed $Ca_{1-x}Sr_xZrO_3$ (x=1) films were shown in Fig. 4. Three main bands are

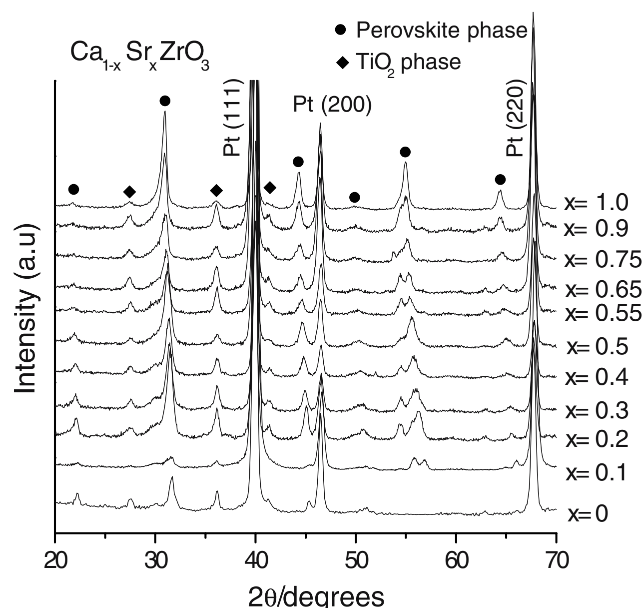

Fig. 3 XRD patterns of $Ca_{1-x}Sr_xZrO_3$ ($0 \le x \le 1$) thin films annealed at 700 °C

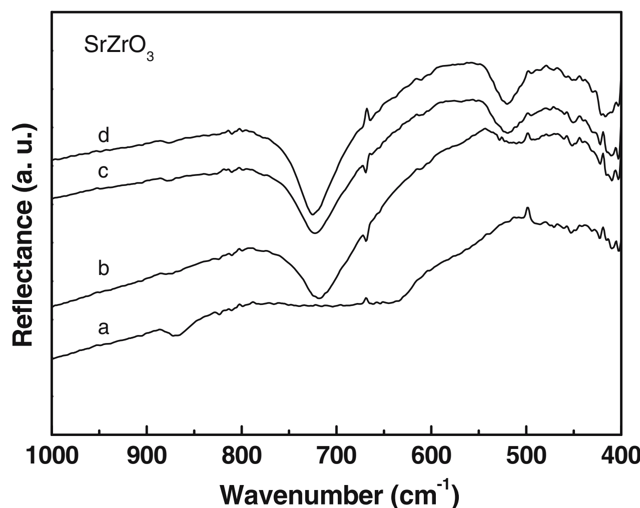

Fig. 4 FT-IR reflectivity spectra at 1000–400 cm^{-1} for $Ca_{1-x}Sr_xZrO_3$ (x=1) films annealed at: **a** 550 °C; **b** 600 °C; **c** 650 °C; **d** 700 °C

clearly shown in the spectra as follows: metal–oxygen (M–O) bonding between 400–800 cm^{-1}, carbon–oxygen (C–O) bonding between 1,300–1,800 cm^{-1}, and entrapped atmospheric CO_2. When the film annealed from 550 to 700 °C, the absorption bands located between 1,800 and 1,300 cm^{-1} are associated with unreacted organic compounds in the films, which typically involve C=O stretching, C–H bending, O–H bending, C=C stretching, and C–O stretching vibrations [13, 14]. The intensities of these absorption bands decreased with the increase of annealing temperature, indicating that the dissociation and evaporation of these metal–organic compounds are occurred. Although the carbonates are not detected by XRD, however, the infrared spectra clearly shows that the residual organic species exist in the samples annealing at low annealing temperature. The further heat treatment is necessary to remove the organic species of residual carbonates in the films and to develop the crystallinity for those films. The reflectance peak around

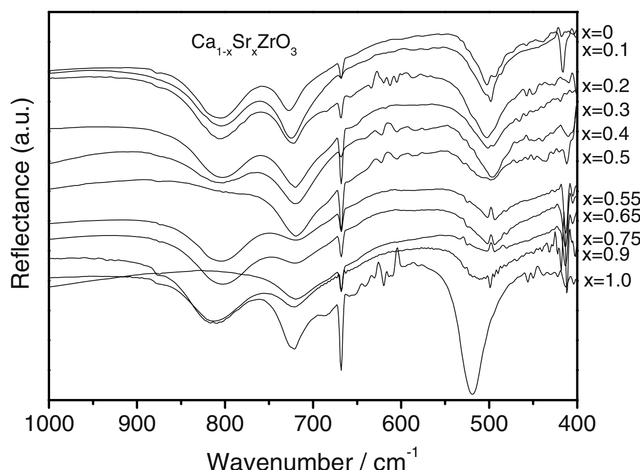

Fig. 5 FT-IR reflectivity spectra at 1000–400 cm^{-1} for $Ca_{1-x}Sr_xZrO_3$ (x=0 to 1) films annealed at 700 °C

Table 1 The surface root mean square roughness (RMS) corresponding to the annealing temperature.

Annealing Temperature (°C)	550	650	800
Root mean square roughness (Å)	12.7	33.88	63.5
Average grain size (nm)	–	–	400

805 cm^{-1} may be attributed to the longitudinal optical phonons of TiO_2, as evidenced by the emerged (002) TiO_2 diffraction peak in Fig. 2. The reflectance peaks at 520 and 724 cm^{-1} may be assigned to ZrO_6 octahedral stretching vibration [15]. All of the FTIR data suggest the complete decomposition of carbonate and the growth of the perovskite phase when the films annealed at above 600 °C.

The systematic infrared reflectance spectra of the $Ca_{1-x}Sr_xZrO_3$ (x=0 to 1) films annealed at 700 °C are shown in Fig. 5. The infrared reflectance peaks between 502 and 520 cm^{-1} are attributed to Zr–O stretching. The infrared-active mode ν_1 at 520 cm^{-1} for $SrZrO_3$, assigned to the Zr–O stretch, shifts to the corresponding mode for $CaZrO_3$ at 502 cm^{-1} decreasing its intensity with x; the 720 cm^{-1} mode for $SrZrO_3$ may be assigned to the Zr–O_6 vibration begins shift to 728 cm^{-1} with x decreasing at $x \leq 0.8$.

The microstructure such as grain size and surface roughness is an important parameter determining the dielectric and electrical properties of thin films. Figure 6 shows the AFM images of the $Ca_{1-x}Sr_xZrO_3$ (x=1) films annealed at different temperatures. The evolution of $SrZrO_3$ samples roughness is listed in Table 1. It is evident that when annealed at 550 °C, the sample showed a homogeneous surface morphology with low roughness, as shown in Fig. 6a. It agrees with the XRD patterns discussed before that the sample annealed at 550 °C has amorphous structure. Fig. 6b shows the surface morphology of the $Ca_{1-x}Sr_xZrO_3$ (x=1) films annealed at 650 °C, the increased root mean square roughness (RMS) indicates that the material's structure becomes increasingly ordered. In addition, the surface morphology changes greatly after annealed at 800 °C (see Fig. 6c). At this stage of growth, coalescence of grains occurs, with the formation of granular structures resulting in a significant increase of roughness.

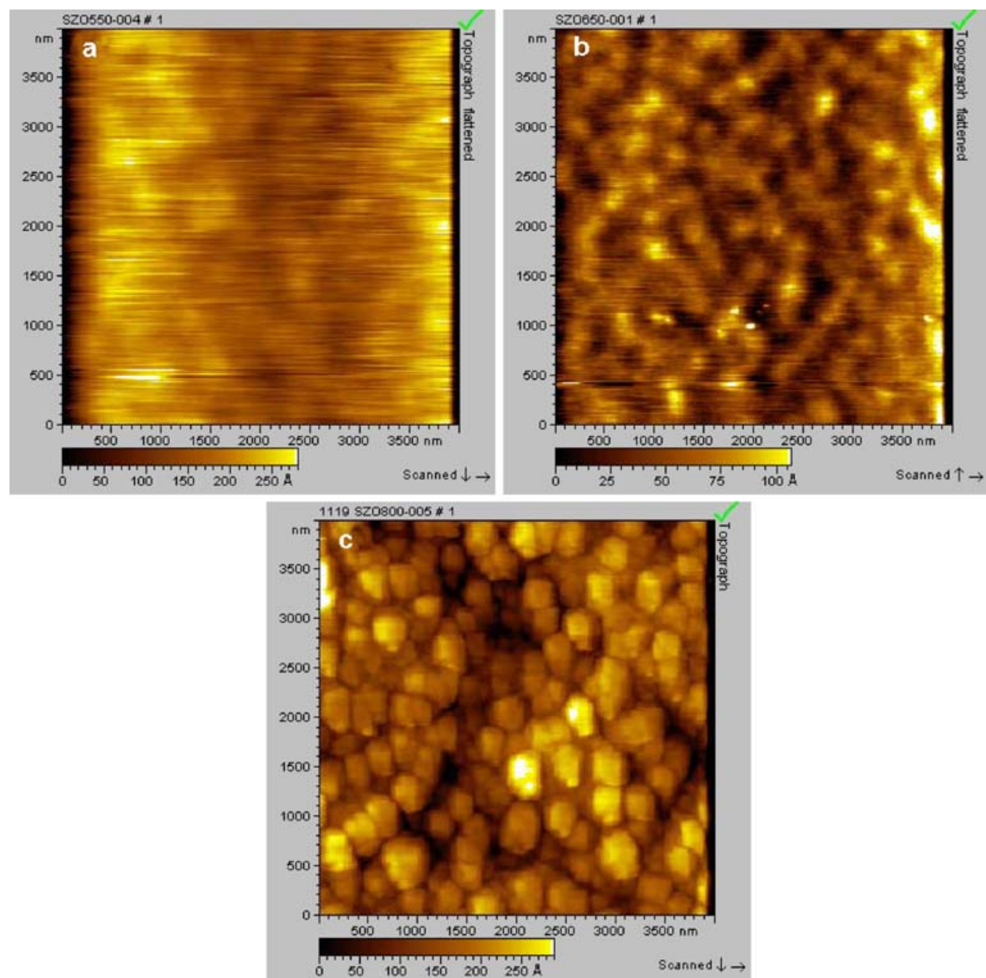

Fig. 6 AFM micrographs of the $Ca_{1-x}Sr_xZrO_3$ (x=1) films annealed at: **a** 550 °C; **b** 650 °C; **c** 800 °C

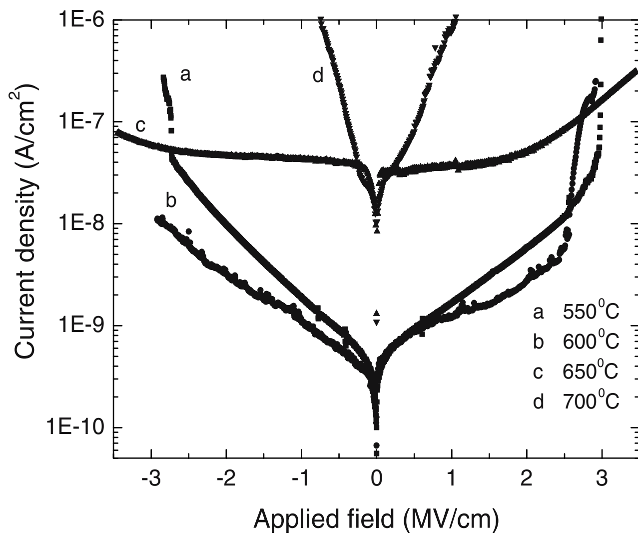

Fig. 7 Leakage current density dependence on applied field of the $Ca_{1-x}Sr_xZrO_3$ (x=0) films annealed at different temperatures for 1 h in O_2

The leakage current density vs. electric field characteristics for MIM capacitors Au/Ti/$CaZrO_3$/Pt of those films annealed at different temperatures are shown in Fig. 7. Two regimes may be distinguished in the *I–V* characteristic. At very low electric fields, the current density increases approximately linearly with voltage, which attributes to dielectric relaxation, the samples display nearly Ohmic behavior. This current would be due to the hopping conduction mechanism in a low electric field, because the thermal excitation of trapped electrons from one trap site to another dominates transports in the films. At higher fields, the current density is proportional to the square root of the applied electric field, suggesting that the Schottky emission is the dominant conduction process for the sol-gel derived thin films. A leakage current density of 9.5×10^{-8} A/cm^2 at the high applied electrical field of 2.6 MV/cm was obtained for the $CaZrO_3$ thin film annealed at 650 °C for 1 h. Nevertheless, a higher leakage current density for the film annealed at 550 °C than that of film annealed at 600 °C is believed due to the carbonate existing in the film. In addition, for the film post-annealed at 700 °C, the poor leakage property may be attributed to the increase in the grain size thus open grain boundaries in thin films which are annealed at relatively high temperature [16].

The dielectric characteristics of $Ca_{1-x}Sr_xZrO_3$ (x=0) thin films annealed at various temperatures of 550, 600, 650 and 700 °C as a function of frequency measured at room temperature are shown in Fig. 8. During the measurement, the applied voltage was zero and the oscillation level was 50 mV. The flat curves indicating the dielectric constants dependence of the sweeping frequency, exhibit very little dispersion of the dielectric constants for these films in a frequency range from 100 Hz to 1 MHz. The dielectric loss is very low for the samples annealed in O_2.

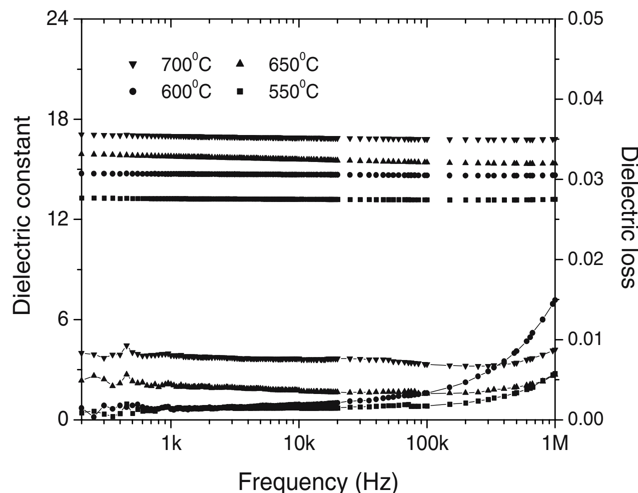

Fig. 8 Dielectric constant and dielectric loss dependence on frequency of the $Ca_{1-x}Sr_xZrO_3$ (x=0) films annealed at different temperatures in O_2

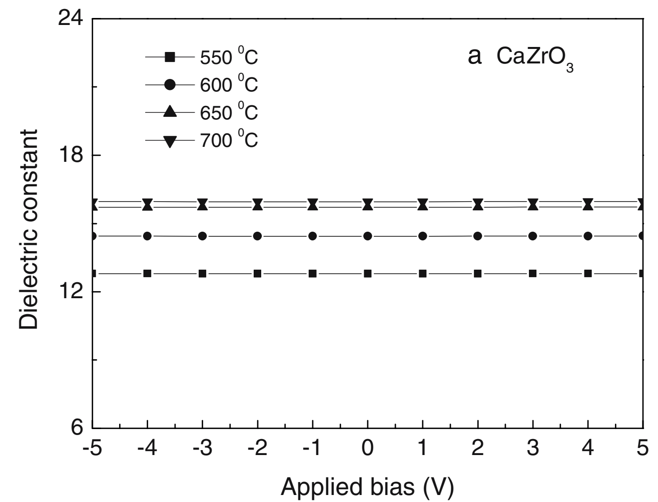

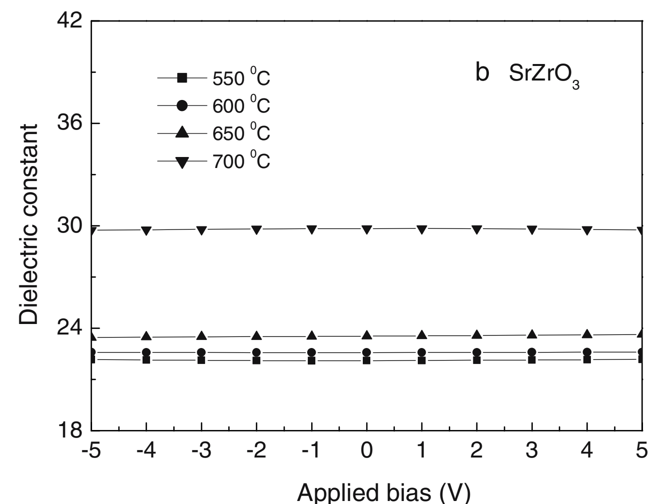

Fig. 9 Dielectric constant dependence on applied bias of the **a** $Ca_{1-x}Sr_xZrO_3$ (x=0) and **b** $Ca_{1-x}Sr_xZrO_3$ (x=1) films annealed at different temperatures in O_2

The high frequency $C–V$ traces at 100 kHz for MIM capacitors were measured at room temperature. Figure 9a and b shows the dielectric constants dependence on the applied bias for the $Ca_{1-x}Sr_xZrO_3$ (x=0) and $Ca_{1-x}Sr_xZrO_3$ (x=1) samples annealed at various temperatures of 550, 600, 650 and 700 °C in O_2 flow for 1 h. The flat curves with no any significant change in dielectric constant clearly show that the dielectric constant of these samples does not depend on the applied bias. At the frequency of 100 kHz, the respective values of dielectric constants for $CaZrO_3$ films annealed at 550, 600, 650 and 700 °C are 12.8, 14.4, 15.7 and 16.0, and the corresponding values of dielectric loss are 0.0018, 0.0027, 0.0026 and 0.0027, respectively; the dielectric constants for $SrZrO_3$ films annealed at 550, 600, 650 and 700 °C are 22.0, 22.6, 23.3 and 28.7, and the corresponding values of dielectric loss are 0.0023, 0.0018, 0.0047 and 0.0026, respectively. The values of dielectric constant in a range of 16–30 for $Ca_{1-x}Sr_xZrO_3$ thin films have been obtained. All the other $Ca_{1-x}Sr_xZrO_3$ films with different x compositions show the similar dielectric properties with these two end member samples. In most cases, the capacitor devices require that there is no practical change in the value of capacitance with the change in electric field. Thus, the $Ca_{1-x}Sr_xZrO_3$ films are suitable for capacitor in practical high-k device use.

4 Conclusion

In this paper, perovskite $Ca_{1-x}Sr_xZrO_3$ dielectric thin films have been obtained using the sol-gel process, and characterized their structural, dielectric and electric properties using a variety of techniques. XRD, FTIR, AFM analysis have demonstrated that the film annealed at 550 °C is amorphous with existing of carbonates, while the carbonates and other organics are decomposed and the film crystallized into perovsite phase at 600 °C and above. Dielectric results show that those films exhibit stable dielectric properties nearly independent on the applied electrical field and frequency at room temperature. The high dielectric constant, low leakage current density and stable dielectric properties suggest that the $Ca_{1-x}Sr_xZrO_3$ dielectric thin films are a promising candidate material system for high-k microelectronic devices applications.

References

1. D.A. Buchanan, S.H. Lo, Microelectron. Eng. **36**, 13 (1997)
2. R.A. Davies, M.S. Islam, J.D. Gale, Solid State Ion. **126**, 323 (1999)
3. S. Yamaguchi, K. Kobayashi, T. Higuchi, S. Shin, Y. Iguchi, Solid State Ion. **136–137**, 305 (2000)
4. N.L. Ross, T.D. Chaplin, J. Solid State Chem. **172**, 123 (2003)
5. H.S. Potar, S.B. Deshpande, A.J. Patil, A.S. Deshpande, Y.B. Khollam, S.K. Date, Mater. Chem. Phys. **65**, 178 (2000)
6. J.R. Hellmann, V.S. Stubican, J. Am. Ceram. Soc. **66**, 260 (1983)
7. V.S. Stubican, J.R. Hellmann, Mater. Sci. Monogr. **10**, 257 (1982)
8. T. Nishino, Nippon Kagaku Kaishi, **10**, 1681 (1981)
9. R.C. Garvie, J. Am. Ceram. Soc. **51**, 553 (1968)
10. V.S. Stubican, S.P. Ray, J. Am. Ceram. Soc. **60**, 534 (1977)
11. M.-H. Yeh, K.-S. Liu, I-N. Lin, Jpn. J. Appl. Phys. **34**, 2447 (1995)
12. J.P. Wang, Y.C. Ling, M.H. Yeh, K.S. Liu, I.N. Lin, Appl. Phys. Lett., **68**, 3401 (1996)
13. R.L. Pecsok, L.D. Shields, *Modern Methods of Chemical Analysis* (Wiley, New York, 1968)
14. A.T. Schwartz et al., *Chemistry in Context*, (American Chemical Society, Washington, DC, 1994)
15. W. Zheng, W. Pang, G. Meng, Solid State Ion. **126**, 323 (1998)
16. W. Zhu, O.K. Tan, X. Yao, J. Appl. Phys. **84**, 5134 (1998)